

VeRNA1: A Tool for Mining Fuzzy Network Motifs in RNA

Carlos Oliver * † ‡, Vincent Mallet * § ¶, Pericles Philippopoulos ||, William L. Hamilton † ‡ and Jérôme Waldispühl §

† *School of Computer Science, McGill University*

‡ *Montreal Institute for Learning Algorithms*

§ *Structural Bioinformatics Unit, Pasteur Institute*

¶ *CBIO, Les Mines-Paristech*

|| *Department of Physics, McGill University*

* *Both authors contributed equally*

ABSTRACT

Motivation : RNAs are ubiquitous molecules involved in many regulatory and catalytic processes. Their ability to form complex structures is often key to support these functions. Remarkably, RNA 3D structures are articulated around smaller 3D sub-units referred as RNA 3D motifs that can be found in unrelated molecules. The classification of these 3D motifs is thus essential to characterize RNA structures, but current methods can only retrieve motifs with identical base interaction patterns.

Results : Here, we relax this constraint by posing the motif finding problem as a graph representation learning and clustering task. This framing takes advantage of the continuous nature of graph representations to model the flexibility of RNA motifs while retaining the convenient encoding of RNAs as graphs. We propose a set of node similarity functions, clustering methods, and motif construction algorithms to recover flexible RNA motifs. We show that our methods are able to retrieve and expand known classes of motifs, but also to identify new motifs. Our tool, VeRNA1 can be easily customized by users to desired levels of motif flexibility, abundance and size.

Availability and Implementation : The source code, data and a webserver are available at vernal.cs.mcgill.ca

Contact : jeromew@cs.mcgill.ca

Supplementary Information : All supplementary files are available online

1. Introduction

Non-coding functions of ribonucleic acids (RNAs) are frequently determined by their 3D structure and folding dynamics [1]. The linear chain of nucleotides (A, U, C, G) builds first canonical (Watson-Crick and Wobble) and non-canonical (all the others) base pairs [2], which serves as a scaffold for the formation of the full tertiary structure. The conservation of these base pairs is thus essential to preserve the folding properties of the RNA and offers a robust signature for the functional classification of RNAs [3].

The comparison of experimentally determined RNA structures revealed the occurrence of highly similar 3D sub-units, called RNA 3D motifs, that are characterized by similar base pair networks and repeated across unrelated RNA [4]. A complete library of RNA 3D motifs would be a valuable source of information for evolutionary studies and also boost structure prediction methods.

Efficient and automated methods to compare databases of RNA structures are essential to achieve this goal [5], [6], [7]. Their results contributed to the advancement of sequence-structure prediction tools [8], [9], and showed promises for interpreting of function prediction algorithms based on RNA 3D networks [10].

1.1. Related Work

RNA motif mining methods can be broadly classified in two categories: 3D-based and graph-based. 3D-based tools seek to identify families of related structures by performing alignments and clustering of *atomic coordinates*. RNA3dmotifAtlas [7], RNA Bricks [11], and RNA MCS [12] illustrate this approach. Since similarity can be conveniently defined directly in Euclidean space for atomic coordinates, the notion of structural proximity of motifs identified by these tools naturally accommodate some degree of variability. However, these methods require a decomposition of RNA into rigid sub-units to be compared to each other (i.e., comparing all internal loops to each other), which limits the scope of possible motifs to be found.

On the other hand, network-based tools aim to identify similarities at the base pairing level. This approach is computationally more efficient and effective because the base pair networks provide a robust signature of the 3D structure. More formally, for any RNA 3D structure (set of atomic coordinates) we can build a multi-relational graph where nodes correspond to nucleotides and base pairing edges are labeled with one of 12 possible nucleotide pairing geometries, as described in Westhof et al. [2]. In this set of 12 geometries, we can find the standard Watson-Crick (A-U, C-G, G-U) pairs, also known as “canonical base pairs”, which are the most abundant class. However, when interpreting 3D motifs, the remaining 11 geometries, also known as “non canonical” are typically of great interest [2]. Covalent connections between nucleotides are assigned a non-base pairing edge type. The edge labels are thus a discretization of relative spatial orientation of the paired nucleotides and provide information close to the true 3D geometry.

Of course, identifying motifs requires a combinatorial search and thus strong limitations on the common subgraph mining have to be imposed. Among these is the ability to include variability within motifs (non-isomorphic instances of the same motif). RNA3dmotif [5] was among the first to propose a solution by searching for exact motifs only within certain known structural elements. More recently, CaRNAval [6] attempted to expand the class of motifs by considering interactions that connect multiple secondary structure

elements and proposing various heuristics, again only retrieving isomorphic motif instances.

The notion of a flexible motif has been very well studied in the sequence domain [13] where certain DNA sequences are accepted to be related while their nucleotide composition can vary. Not surprisingly, the same applies in the RNA structural domain where well-known motifs such as the A-minor are known to admit variability in their connectivity pattern [14], and thus methods which rely on strict isomorphism would fail to identify such instances, as well as miss motifs entirely. Indeed, none of these methods conduct searches for motifs occurring in any context, while at the same time allowing for flexibility in the motifs found.

1.2. Contributions

In this work, we leverage the state of the art in graph representation learning to build continuous embeddings of RNA structures and identify structurally conserved yet variable neighborhoods. We then propose two algorithms leveraging these graph representations to perform graph queries and identify novel motifs. We are able to retrieve known and novel instances of existing motifs. Using our second algorithm, we are able to infer novel motifs, while also identifying established ones.

2. Datasets

We extract motifs from the set of experimentally determined RNA crystal structures [15]. To ensure that the frequency of a motif is not biased by redundant crystal structures, we use the representative set at 4 Angstroms provided by BGSU [7]. We then build RNA networks for each RNA using the FR3D annotations provided by the same framework. This results in a total of 1297 RNAs and 671232 nodes (nucleotides). In order to achieve approximately constant batch sizes at training time, our training set consists of chopped graphs in constant chunks of RNA of approximately 50 nucleotides, as is detailed in **Supplementary Algorithm 4**. Once the model is trained we perform all motif finding operations on the whole graphs. Our validation sets consist of motifs identified by RNA 3D Motif Atlas [7], RNA3dmotif [5], and CaRNAval [6].

3. Methods

We introduce V_{eRNA1} , an algorithm that first decomposes RNA networks into small structural building blocks of RNA and then aggregates these blocks based on their co-occurrence in the graphs. The extraction step introduces custom structural comparison functions (Section 3.2) which are used to build a space of continuous embeddings for efficient clustering (Section 3.2.2). Finally we introduce a custom Graph Edit Distance for RNA to use as a metric for model selection and evaluation (Section 3.2.3).

We then combine information from the embedding space and connectivity in the graph space into a meta-graph data structure (Section 3.3). We leverage this data structure to retrieve graphs similar to a query (Section 3.4), and to streamline frequent substructure searches and thus identify *fuzzy* motifs (Section 3.5).

3.1. Problem Definition

We start with a set of multi-relational graphs $\mathbb{G} = (\mathbb{V}, \mathbb{E})$ (whole RNA structures) as described above. We define a motif as a set of subgraphs $\mathcal{M} = \{g_1, g_2, \dots\}$, drawn from \mathbb{G} , such that the following properties hold:

- 1) *Similar*: For any pair $(g_i, g_j) \in \mathcal{M}$, $\text{SIM}(g_i, g_j) \geq \gamma$, where SIM is a similarity function on graphs. We allow the user to set γ .
- 2) *Connected*: $\forall g_i \in \mathcal{M}$. g_i is a connected subgraph.
- 3) *Frequent*: the number of subgraphs of \mathcal{M} should be above some user-defined threshold : $|\mathcal{M}| > \delta$

The motif finding problem is thus to identify all motifs \mathcal{M} that fit the above criteria. An exact solution to this problem would imply enumerating all subsets (search for subgraphs) of \mathbb{G} and ensuring that these criteria are satisfied (compare graphs). In the most general case, both procedures admit exponential time algorithms [16]. Previous works set $\gamma = 1$, so that the similarity constraint becomes another graph problem, known as the maximal graph isomorphism problem [6]. Additionally, the search step is often also limited by considering only certain substructures. Here, we allow for non-identity γ (fuzziness) and search remove constraints on secondary structure context [6], [7].

3.2. Rooted Subgraph Embeddings

Recent advances in Graph Representation Learning provide efficient tools for embedding structural objects in Euclidean space [17]. This allows us to naturally encode the notion of structural similarity and perform efficient comparisons necessary for identifying fuzzy motifs. More formally, given a parametric function $\phi : u \rightarrow \mathbb{R}^d$ (typically a graph neural network) which maps elements u of a graph (nodes, edges, subgraphs, or whole graphs) to real vectors, and a similarity function s_G on these objects, we can train ϕ via backpropagation to approximate s_G (Equation 2).

In this manner, the output of the model is an embedding (or representation) of a graph element in Euclidean space, such that distances in this space reflect distances in the graph space in which s_G operates. Conveniently, while s_G can be expensive to compute, the resulting feature map ϕ , once sufficiently trained, acts inductively and can be cheaply applied to new data [18].

3.2.1. Rooted Subgraph Comparisons. Since motifs can be subgraphs of arbitrary size, we first decompose \mathbb{G} into fundamental units on which we apply ϕ and then reconstruct larger motifs. We choose to decompose \mathbb{G} as a set of rooted subgraphs centered at individual nucleotides. A rooted subgraph g_u is the induced subgraph on the set of nodes $u' \in g$ such that $d(u, u') \leq r$ where d and d is the shortest length path between two nodes, and r is a user-defined threshold. This is a natural building block of RNA structure which allows for reconstruction of any structural motif.

We note that for RNA motifs, we are only interested in considering edge type, and graph structure, and ignore any node information (this can be easily introduced if needed). Notably, it is known that certain relation types (base pairing geometries) share structural similarities. Stombaugh [19] computed the geometric discrepancy between all pairs of relation types. This phenomenon is known as isostericity (Shown in **Figure A.8**). In order to perform fast comparisons and clustering of rooted subgraphs, we introduce various similarity functions which induce a continuous notion of structural similarity.

Here, we define a similarity function between a pair of rooted subgraphs, g_u and g_v . The function s_G operates on the output of a function $f : u \rightarrow \Omega$ which decomposes a rooted subgraph into a set of objects Ω . These can be a set of nodes, edges, or smaller subgraphs such as graphlets [20]. These objects can then be assigned structural and locality compatibilities. We let $\mathbf{C}_{\omega, \omega'}$ be the structural compatibility between objects ω, ω' , for example, edge isostericity. Next, $\mathbf{D}_{\omega, \omega'}$ assigns a cost on pairs of objects depending on the relative path distance to their respective root

nodes. We propose various similarity functions, based on optimal matching of these objects with the most general form being:

$$s_G(g_u, g_v) := \min_{\mathbf{X}} \sum_{\omega \in \Omega} \sum_{\omega' \in \Omega'} (\alpha \mathbf{C}_{\omega, \omega'} + \beta \mathbf{D}_{\omega, \omega'}) \mathbf{X}_{\omega, \omega'} \quad (1)$$

where \mathbf{X} is a binary matrix describing a matching from the elements of Ω to Ω' , α and β are user-defined weights for emphasizing locality vs structural compatibility. We solve for the optimal matching between two sets of structural objects using the Hungarian algorithm [21]. All our similarity functions are described in detail in Supplementary Section C.

3.2.2. Model Training. In order to identify related groups of rooted subgraphs using a only the similarity function we would have to perform and store N^2 operations. When working with an order of 10^7 nodes, this quickly becomes prohibitive. Once nodes in each graph are embedded into a vector space, searches and comparisons are much cheaper as they are vector operations.

We therefore approximate the s_G function over all pairs of rooted subgraphs using node embeddings $\mathbf{Z} \in \mathbb{R}^d$ with a learned feature map. We use a Relational Graph Convolutional Network (RGCN) model [22] as parametric node embedding function $\phi(u) \rightarrow \mathbb{R}^d$ which maps nodes to a vector space. The network is implemented in Pytorch [23] and DGL [24]. Given a similarity matrix K induced by s_G , this function is trained to minimize :

$$\mathcal{L} = \|\langle \phi(u), \phi(v) \rangle - K(u, v)\|_2^2, \quad (2)$$

To make embeddings more focused on subgraphs that contain non canonical nodes and avoid the loss to be flooded by the canonical interactions (Watson Crick pairs), we then scale this loss based on the presence of non canonical interactions in the neighborhood of each node being compared. Given the frequency of non canonical interactions f and $\mathbb{1}_u$ an indicator function that denotes the presence of non-canonical interactions in the neighborhood of node u , the scale $s_{u,v}$ of the u, v term writes as :

$$\mathbf{S}_{u,v} = (1 + \frac{\mathbb{1}_u}{f})(1 + \frac{\mathbb{1}_v}{f}), \quad \mathcal{L}_{scaled} = \mathbf{S} \odot \mathcal{L} \quad (3)$$

We can then perform a clustering in the embedding space using any linear clustering algorithm and this yields the aforementioned structural blocks of RNA. We denote such clusters as 1-motifs and plot them in **Figure 3**.

3.2.3. Model Selection: RNA Graph Edit Distance. The choice of similarity function is application specific. One can use a function which maximizes performance on a downstream supervised learning task, or one can choose a similarity function which best encodes structural identity [17]. Since supervised learning data for RNA 3D structures is scarce, we opt for the latter and propose the Graph Edit Distance (GED) (or its similarity analog $exp[-GED]$) between rooted subgraphs, as this is widely accepted yet computationally intensive gold standard for structure comparison [25]. Interestingly, GED is a generalization of the subgraph isomorphism problem [26] which is at the core of previous RNA motif works such as CaRNAval and RNA3dmotif.

In a nutshell, the GED between two graphs g, h is the minimum cost set of modifications that can be made to g in order to make it isomorphic to h . This naturally encodes a notion of similarity since similar pairs will require few and inexpensive modifications, and vice versa. We have adapted this algorithm to RNA data. A detailed description of the algorithm is available in Supplementary Section B. We use the isostericity matrix for edge substitutions, and do not apply a penalty to node substitutions.

Let $\mathcal{E}(\cdot)$ be a function that returns the edge label for a given edge, and ISO the isostericity function which returns the similarity between edge types. We define an RNA cost function over pair of edges p and q as follows :

$$c(p \rightarrow q) = \text{ISO}(\mathcal{E}(p), \mathcal{E}(q))$$

$$c(p \rightarrow \emptyset) = \begin{cases} \alpha & \text{backbone} \\ \beta & \text{canonical} \\ \theta & \text{non-canonical} \end{cases}$$

We propose a simple modification to allow for comparison of rooted graphs (**Algorithm 5**), and use the general version of GED to validate the ultimate full subgraph-level quality of our identified motifs.

3.3. Meta-graph

While there is no limit to the size of a real-world motif, our rooted subgraph embeddings are currently only aware of a fixed-size neighborhood. For this reason, 1-motifs only identify motifs as large as the number of layers in the similarity function/RGCN. However, we can extend these to k -motifs by aggregating several clusters based on co-occurrence in the original graph. This allow us to aggregate heterogeneous rooted subgraphs into larger motifs while preserving the property of co-occurrence.

To guide this aggregation, we introduce a meta-graph data structure \mathcal{G} , whose meta-nodes are composed of regions of the embedding space and whose edge are based on the connectivity in the RNA graphs between those regions. Hence, the meta-graph simultaneously encodes structural proximity and locality in the graph in one object. To get the meta-nodes we simply cluster the original nodes embeddings in \mathbb{V} and use the clusters as meta-nodes : $C_i = \{n \in \mathbb{V}, \text{cluster}(n) = i\}$. The number of clusters and their spread are a parameter that modulates the fuzziness and the sensitivity of the induced methods. We associate to each node its meta-node, or cluster ID, and its distance to the cluster center. Meta-edges $E_{i,j} = \{(n_i, n_j) \in (C_i \times C_j) \cap \mathbb{E}\}$ store the edges in RNA graphs that go from one cluster to another. This process is illustrated in **Figure 1**.

The meta-graph data structure enables an efficient implementation of the following algorithms as well as an easier way to describe and visualize them. Building the meta-graph requires RGCN inference on all nodes and clustering, and iterating through all edges in \mathbb{G} . With linear-time clustering techniques, building the meta-graph is therefore done in time $O(|\mathbb{V}| + |\mathbb{E}|)$.

3.4. Retrieving known motifs

The first use of the meta-graph data structure is to retrieve subgraphs similar to a query subgraph. Such an algorithm could identify subgraphs that resemble known motifs but which were not identified by tools imposing strict isomorphism [27].

The idea of the algorithm is to use the alignment of the RNA graphs induced by the embeddings (**Fig. 1**) to efficiently search for similar structures. Using the RGCN, we place the query graph in the embedding space which creates a query multigraph \mathcal{G}^q whose nodes correspond to specific clusters, and whose edges of \mathcal{G}^q are in line with the connectivity of the query. Since each query node is assigned a specific embedding vector, we can directly obtain a ‘‘score’’ inversely related to the distance between a query and a hit node’s embeddings. In this sense, a ‘‘hit’’ can be any element of the set of all possible connected subgraphs of \mathcal{G}^q . The task then becomes to identify the highest scoring of these subgraphs.

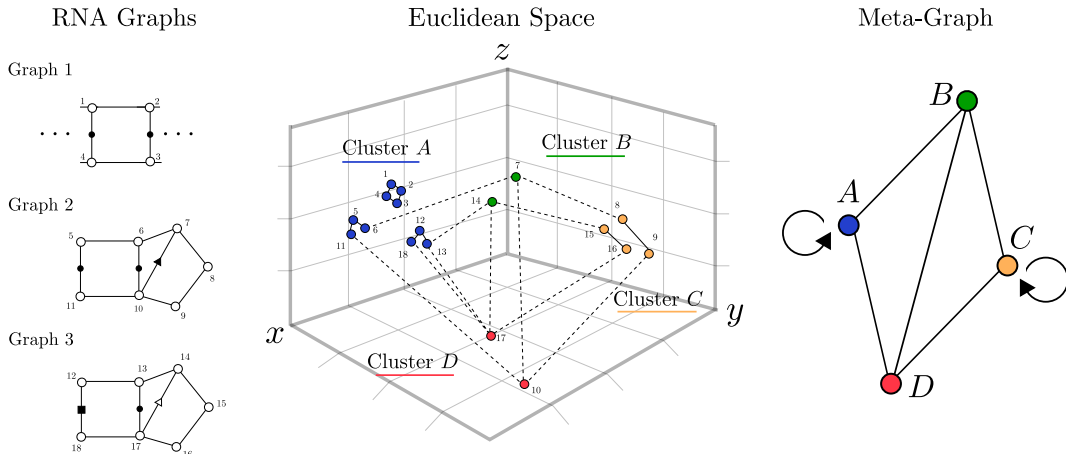


Figure 1: Meta-graph creation : RNA graphs get aligned in the embeddings space. Meta-nodes group the low GED RNA nodes through clustering. We then infer meta-edges from the source graphs connectivity

To get these connected subgraphs, we start from the set \mathcal{M} of all nodes involved in the query. We then iterate through the edges of the \mathcal{G}^1 and try to merge any two elements of \mathcal{M} that fall along the current edge. Merging is not trivial, because the graph is not a geometric one : two meta-nodes linked to the same neighbor are not necessarily connected. We implement a merging algorithm presented in **Algorithm 1** to address this problem. Any merge operation increases the score of the resulting set by summing the score of the merged elements This retrieval procedure is detailed in **Algorithm 2**.

Algorithm 1: Merging Algorithm

Data:

- S : a set of RNA subgraphs.
- Meta-node C , meta-edge E

Result: T , an expanded S to include C through E

```

1  $T \leftarrow \emptyset$ 
2 foreach  $e \in E$  do
3   Get  $g$ , the graph  $e$  is part of.
4   foreach  $set$  in  $g \cap S$  do
5     if  $set \Delta e = node$  then
6        $T \leftarrow T \cup \{set \cup node\}$ 
7     end
8   end
9 end
10 return  $T$ 

```

Finding all relevant clusters and looping through the edges list is facilitated by the meta-graph structure : we can see the successive edge merging as a walk in the meta-graph. If a hit encompasses the full query, it will have undergone the most merging operations and obtain a maximal score. However, if one node is missing or if the structure is a somewhat different, we still retrieve it with a sub-optimal but high score.

The algorithm remains tractable thanks to the sparsity of the meta-graph that allows efficient iteration through edges, efficient set operations to expand motifs and graph-based separation of the candidate hits. A theoretical analysis of the complexity depends

Algorithm 2: Motif Instances Retrieval

Data:

- Meta-graph (C, E) , original RNA graphs (\mathbb{V}, \mathbb{E})
- Query multi-graph \mathcal{G}^q

Result: \mathcal{M} : Motif instances candidates : a set of sets of nodes and their associated scores

```

11  $\mathcal{M} \leftarrow \bigcup_{C \in \mathcal{G}^q} C$ 
12 foreach  $E$  in  $\mathcal{G}^q$  do
13    $C_1, C_2 = E$ 
14    $T_1 \leftarrow \text{merge}(M, C_1, E)$ 
15    $T_2 \leftarrow \text{merge}(M, C_2, E)$ 
16    $\mathcal{M} \leftarrow \mathcal{M} \cup T_1 \cup T_2$ 
17 end
18 return  $\mathcal{M}$ 

```

heavily on both the topology of the meta-graph and of the query-graph and is explained further in Supplementary section F. We can rely on empirical complexity to say that this algorithm runs in an average of 10s on a single core.

3.5. Mining new motifs

We can leverage a similar strategy to the retrieve procedure when mining motifs *de novo*. The basic intuition of our algorithm, Motif Aggregation Algorithm (MAA) is that the set of nodes assigned to a given cluster can be considered to be a motif of cardinality 1 (a 1-motif). We can then use the meta-graph to identify clusters with connections to the current motif set to build larger motifs. Because we lack the guidance of the query, instead of merging just along one edge, we merge along all edges in the meta-graph and filter results based on a user-defined minimal frequency δ .

As an example, starting with a 1-motif e.g. the set of subgraphs in cluster A , we can create 2-motifs by merging each other cluster in its meta-graph neighborhood, $X \in \mathcal{N}(A)$. We then identify of the new 2-motifs from their constituent meta-nodes. This process

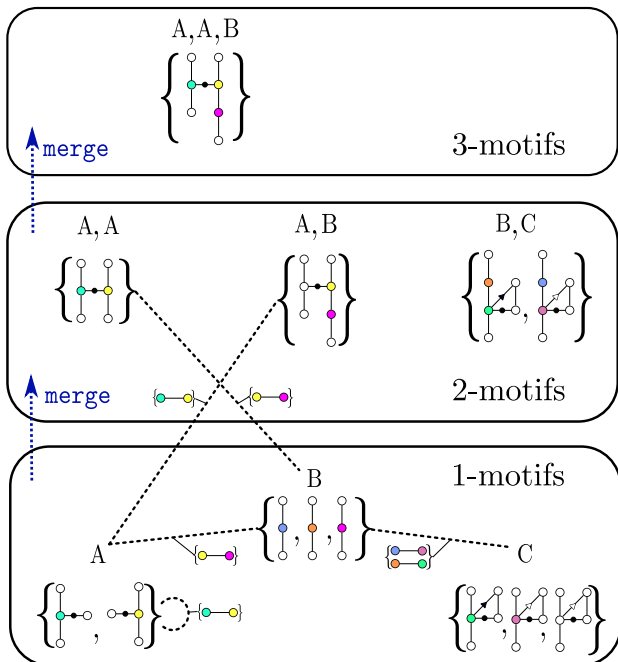


Figure 2: MAA Illustration : Meta-nodes A,B and C get merged into three 2-Meta-nodes AA, AB and BC. Then new meta-edges are computed that link singletons A and B with AB and AA 2-meta-nodes respectively. A second merge follows these links and yields the 3-meta-node AAB. Node colors here are a proxy for node ID, and not tied to the cluster IDs (A, B, C).

can then be iterated to discover k -motifs. This is illustrated in **Figure 2** and outlined in detail in **Algorithm 3**.

At each iteration t , a motif can be extended by a total of $\mathcal{O}(\Delta(G) \times t)$, meta-nodes where Δ yields the maximum degree of the meta-graph. This is because each rooted subgraph in the current motif can potentially form an extending connection. Processing all motifs at a given time step takes $\mathcal{O}\left(\binom{C}{t} \times \Delta(G) \times t\right)$ in the worst case. Of course, in practice the sparsity of the meta-graph limits the growth of the first term since some clusters do not share connections and will thus not be considered as possible extensions. Once all nodes are processed, we can repeat the same search to obtain higher-order motifs. Naturally, as we obtain larger motifs, the number of instances decreases, and the search abandons motifs with number of instances below a user-defined threshold δ . Empirical complexity depends strongly on hyperparameter choices but is on average of a few minutes on a single core.

4. Results

Our tool relies on graph representation methods to drastically improve the scalability of motif mining and facilitate fuzzy matching of motifs. Thus, we first evaluate the quality of our RNA-specific similarity functions and subsequent RGCN-based embedding model (Section 4.1) and show that structural information is faithfully encoded. Following this, we show that our approach can consistently retrieve existing motifs (Section 4.2) while also uncovering new fuzzy motifs (Section 4.3). Throughout the evaluation of the tools, we use GED as an external (and costly) oracle to select a similarity function, assess embedding quality, and motif consistency. We

Algorithm 3: Motif Aggregation Algorithm (MAA). At each step, t , the algorithm iterates through edges (m, m') of the meta-graph, applying Algorithm 1 to construct a $t+1$ motif μ . The updated meta-connectivity is stored as new meta-edges.

Data:

- Meta-Graph \mathcal{G} ,
- Minimum density δ
- Number of steps T

Result: List of meta-graphs

```

19  $\mathcal{M} \leftarrow list()$ 
20  $\mathcal{E} \leftarrow \mathcal{G}.edges()$ 
21 foreach  $t \in \{1, \dots, T\}$  do
22    $\mathcal{E}' \leftarrow \emptyset$ 
23    $\mathcal{M}[t] \leftarrow list()$ 
24   while  $\mathcal{E}$  do
25      $m, m' \leftarrow \mathcal{E}.pop()$ 
26      $\mu \leftarrow merge(m.subgraphs, m', (m, m'))$ 
27     if  $|\mu| > \delta$  then
28        $\mathcal{M}[t].append(\mu)$ 
29       /* Connect new node to
30          adjacent clusters */
31       foreach  $c' \in G.Nei(\mu)$  do
32          $\mathcal{E}'.add((\mu, c'))$ 
33       end
34     end
35    $\mathcal{E} \leftarrow \mathcal{E}'$ 
36 end
37 return  $\mathcal{M}$ 

```

emphasize that the focus of subsequent analysis is on the soundness of the tool, and in-depth biological interpretation of discovered motifs is left for future work.

4.1. Subgraph Comparisons and Embeddings Correlate with GED

We sample 200 rooted subgraphs of radius 1 and 2 uniformly at random from \mathbb{G} . We recall that the radius of a graph is the maximum length shortest path between any two nodes in this graph. Next, we compute all-to-all GED on this sample, yielding 200,000 non trivial values for each radius. We then compute similarities on the same set of subgraphs using various choices of s_G and ϕ . In **Table 1** we summarize the resulting Pearson correlation values.

Under these metrics, the best performing method is the *graphlets* + *hungarian* methods with an almost perfect correlation at a radius of one and 0.52 at a radius of two. When computing the same correlation on pairs of graphs with low GED to each other ($r_{\text{threshold}}$), we obtain higher correlations of 0.637 on the radius-two subgraphs. Since we consider fuzzy motifs to consist of graphs with slight variations such metrics are more relevant.

Thus we train an RGCN using the *graphlet* + *hungarian* similarity function and measure the agreement between embeddings and GED. A correlation value of 0.74 for the thresholded 2-layers RGCN embeddings enables us to claim that the dot product in the embedding space approximates well the structural similarities especially between similar subgraphs. We even obtain better results

| method | depth | decay | normalization | r | r_threshold | r_nc | r_nc_threshold | time (s) |
|----------------------|-------|-------|---------------|-------|-------------|-------|----------------|----------|
| edge hist. | 1 | 0.300 | None | 0.633 | 0.627 | 0.320 | 0.334 | <0.001 |
| edge hist. + iso | 1 | 0.500 | None | 0.769 | 0.783 | 0.526 | 0.533 | <0.001 |
| edge hungarian + iso | 1 | — | None | 0.791 | 0.800 | 0.612 | 0.612 | <0.001 |
| graphlets hist. | 1 | 0.800 | None | 0.967 | 0.973 | 0.948 | 0.962 | 0.029 |
| graphlet hungarian | 1 | — | sqrt | 0.996 | 0.997 | 0.992 | 0.995 | 0.030 |
| graphlet hungarian | 2 | — | sqrt | 0.568 | 0.637 | 0.437 | 0.518 | 0.433 |
| 1hop RGCN | 1 | — | — | 0.919 | 0.990 | 0.783 | 0.931 | <0.001 |
| 2hop RGCN | 2 | — | — | 0.540 | 0.737 | 0.375 | 0.595 | <0.001 |

TABLE 1: Correlation with the GED for different kernels and embedding settings

| Method | Success Rate | Relative ratio in the hit list |
|-------------|--------------|--------------------------------|
| True query | 0.89 | 0.18 |
| Decoy query | 0.15 | 0.92 |

TABLE 2: Comparison of the performance of the retrieve algorithm when used with a query instance vs. a random one.

for the 2-hop version, which can be explained by regularization of the learned model over inputs where the similarity values and the GED were very different. Moreover, we note that the run time of a comparison becomes negligible, as it amounts to a dot product. Full results are available in **Supplementary Table A.5**.

We complete our report of the performance assessment of the embeddings with a visual representation of the results. In **Figure 3**, we generate a 2D projection of the local RNA structures from the learned embedding with t-SNE [28]. We draw example subgraphs corresponding to a sample of clusters.

Visually, we observe that similar subgraphs lie in the same clusters. Additional quantitative metrics are provided in the Supplemental Section E. This validation provides us the structural building blocks to assemble and retrieve motifs.

4.2. Retrieval Algorithm Expands Known Motifs

Next, we turn to the validation of the retrieval algorithm. Given a query graph, the retrieve algorithm returns a list of subgraphs in decreasing order of compatibility to the query, also known as “hits”. We run the algorithm on a selected set of motifs in RNA3dMotifs [5], filtered for sparsity (more than 3 instances) and size (more than 4 nodes). For a given known motif, we perform a retrieve with two types of queries: a true instance of the motif, and an instance of a randomly chosen motif (decoy). We show in **Table 2** the resulting ranks.

We see that when queried with one instance, the algorithm retrieves other instances in 90% of the cases. Annotation errors can sometimes result in instances having different graphs and thus in some cases the instance is not retrieved. However, when queried with a decoy, the success rate drops to 15% with an average rank at the 92nd percentile of the hit list, indicating that only very partial solutions were retrieved.

We can go further by analyzing the structure of the retrieved hits. A first way to do so is to plot several hits with increasing ranks (**Figure 4**). A more quantitative way to do this is to compute the mean GED value of hits at fixed ranks compared to their respective queries. The results are presented in **Table 3**.

A visual inspection of the results indicates that the retrieved graphs differ more and more as we plot hits with decreasing scores. This quantitative experiment validates this result and indicates that on average the ten first hits are almost isomorphic, and even the

| Rank | 1st | 10-th | 100-th | 1000-th | Random Other |
|----------|-----------|-----------|-----------|-----------|--------------|
| Mean GED | 1 ± 2 | 1 ± 2 | 2 ± 2 | 6 ± 4 | 19 ± 7 |

TABLE 3: Mean GED values between several queries and their hits at fixed ranks. We also included mean GED values to other random motifs as a control.

100 first ones are often very similar. Based on both of these results we claim that our method is able to retrieve sets of subgraphs where the GED to the query correlates with the retrieval rank.

The average number of instances of a motif across RNA3dMotif, RNA 3D Motif Atlas, and CaRNAval is only 22.3. Interestingly, the fact that we are able to obtain up to 100 hits with a GED below 2 indicates that many of these represent an ensemble of highly similar structures that are missed by existing tools. This observation suggests that our method can not only be used to assess if we find known instances of a motif, but also to identify fuzzy instances of these well known motifs.

4.3. MAA Identifies Novel Fuzzy Motifs

Finally, we assess the quality of the MAA procedure to identify *de novo* motifs. Of course, there are many choices of hyperparameters which are ultimately application-dependent (fuzziness, motif frequency, size, etc.). We select the number of clusters according to the Silhouette Score and several clustering metrics (See **Figure A.11**) and require a minimum frequency of 100 instances per motif, as well as a maximum cluster spread of 0.4 in units of euclidean distance. We obtain a set of 1,665 motifs up to cardinality 6. **Supplementary Table A.7** shows the average number of instances and number of motifs at each cardinality. To check for internal consistency, we compute the intra- and inter-motif GED between a random sample of 20 motifs and plot the results in **Figure 5**. We obtain an intra-motif GED of 2.0 ± 3.1 and an inter-motif GED of 6.9 ± 2.9 when comparing motifs of the same size. This shows that VeRNA1 finds motifs with internal consistency.

Next, we measure the degree to which our motif set agrees with existing motif databases. In **Figure 6**, we plot the percentage of the known motif’s nodes (RNA 3D Motif Atlas (BGSU), CaRNAval, and RNA3DMotif) that can be found in any of our motifs of the same size. We find that a subset of our motifs aligns well (at least 60% overlap) with all databases (**Table 4**). At the same time, the VeRNA1 motifs that match known motifs feature many more instances, again suggesting that we are able to expand the set of known motif instances.

Finally, we find that 1,148 of our 1,665 motifs do not have any overlap with known motifs, indicating that our algorithm is uncovering novel motifs. An in-depth analysis of all individual instances is out of the scope of this contribution, but we plot a few examples in **Figure 7**. Nonetheless, all the motifs identified

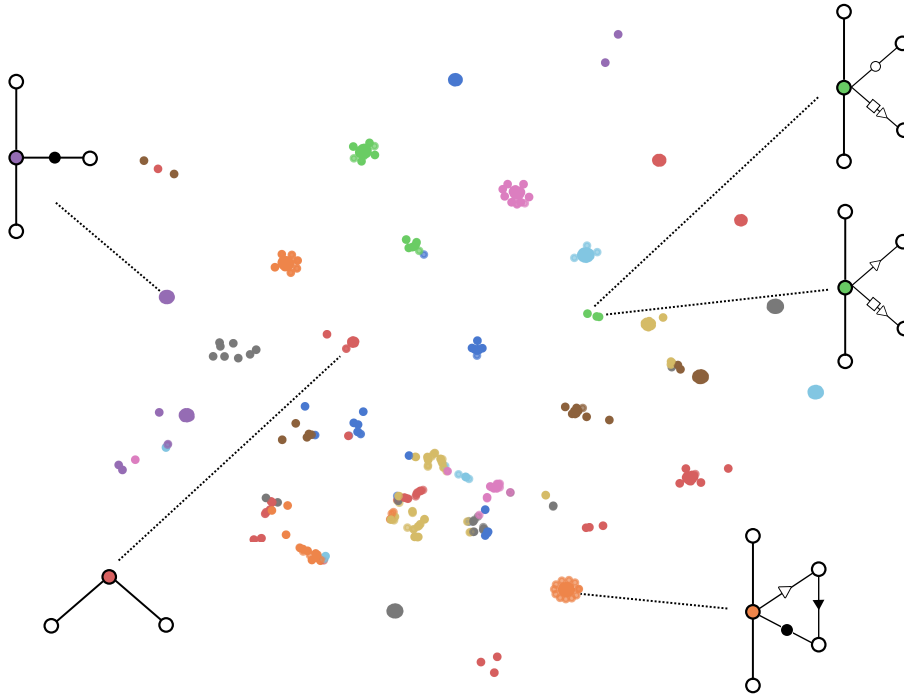


Figure 3: t-SNE projection applied to embedding space. Drawn rooted subgraphs correspond to an example from the cluster connected by a dotted line. Point colors correspond to the nearest mixture model component.

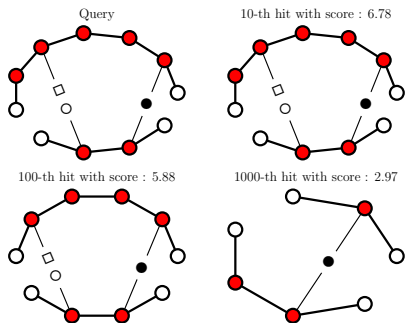


Figure 4: Hit graphs with increasing rank to the query.

| Dataset | Covered | Missed |
|----------------|---------|--------|
| BGSU [7] | 60 | 13 |
| RNA3DMotif [5] | 8 | 2 |
| CaRNAval [6] | 89 | 19 |

TABLE 4: Nearly all motifs identified by three published RNA motif tools are a subset of the motifs found by VeRNAL.

by VeRNAL can be browsed and downloaded on our web server vernal.cs.mcgill.ca, and thus available to the community for further analysis.

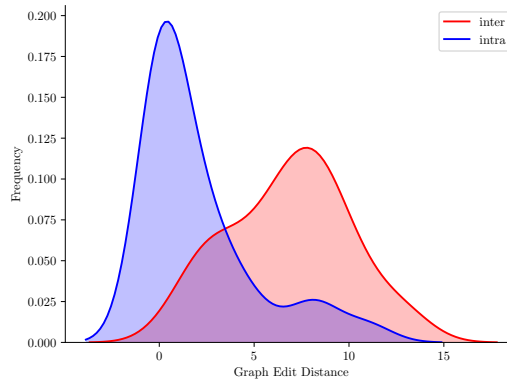


Figure 5: Structural similarity (computed with full Graph Edit Distance) is significantly higher for subgraphs within the same motif compared to subgraphs in different motifs.

5. Conclusions

We describe VeRNAL, a novel pipeline for identifying fuzzy network motifs. We develop various node structure comparison functions and approximate their feature map using an RGCN, embedding our graph dataset to a vector space for fast similarity computation between rooted subgraphs. We show that these computations correlate well with the RNA GED while being significantly faster. This enables us to find small structural building blocks of RNA and organize them into a meta-graph data structure.

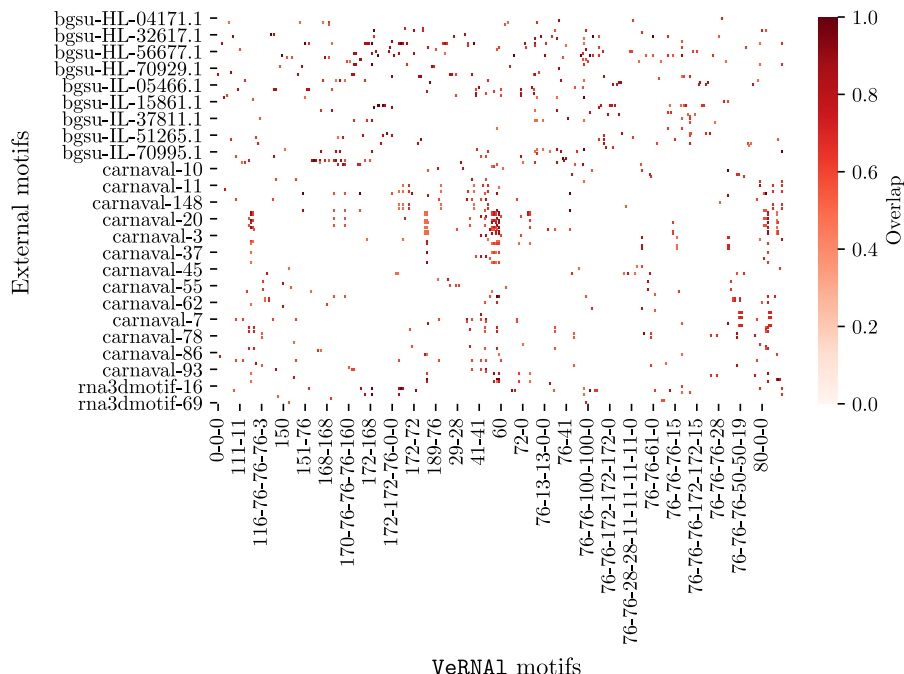


Figure 6: Agreement with existing motif libraries. Each cell value ranges from 0 to 1, where 1 indicates that all the nodes of an instance of a known motif are contained in a `verNAL` motif.

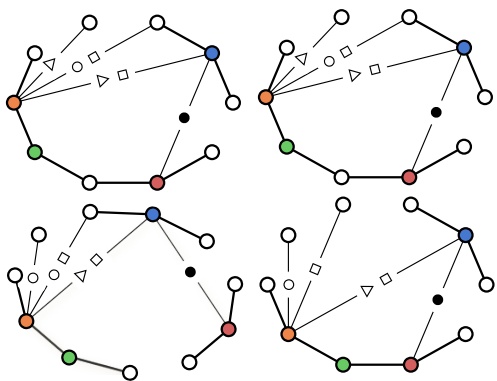


Figure 7: Four instances of a `verNAL` 4-motif motif that did not overlap with external motifs. Each root node’s color corresponds to its cluster ID.

Using this custom data structure, we introduce two algorithms to retrieve similar instances to a known query and to discover new motifs. We show that the retrieval procedure enables us to efficiently identify other instances of known motifs but also to find sets of subgraphs similar but not identical to a query. The motif extraction algorithm is also successful in mining sets of subgraphs with low intra-cluster GED, re-discovering and expanding known motifs as well as introducing new ones. All together, our platform `verNAL` is the first tool to propose fuzzy graph motif extraction.

There are some limitations to `verNAL` which can be addressed in the future. Since RGCNs perform convolutions of entire neighbourhoods, motifs without a wide-enough conserved core can be

lost. Additionally, the motif building algorithm accepts all connected subgraphs belonging to a specific *set* of clusters as instances of the same motif. While the specific manner in which root nodes are connected is not explicitly constrained, this can lead to instances of the same motif with very different topologies. Additional graph-level hashing [?] can eventually be used to distinguish these cases, or using larger embedding radius can mitigate the effects.

The main focus of this work is to build and validate the algorithm. Yet, a detailed exploration of the candidate motifs and the impact of the hyperparameters (fuzziness, density, size, etc.) should be explored in future work.

The algorithms introduced here are general and the field of subgraphs mining is still rapidly evolving. We believe `verNAL` could also be applied to other sources of data such as chemical compounds, protein networks, and gene expression networks to automatically mine for novel generalized structural patterns.

6. Implementation

The source code is available at vernal.cs.mcgill.ca. We also provide a flexible interface and a user-friendly webserver to browse and download our results.

7. Acknowledgements

The authors thank Vladimir Reinharz, Yann Ponty, Roman S. Gendron and Jacques Boitreaud for advice and support.

8. Funding

C.G. was funded by a PhD scholarship from Fonds de Recherche du Québec Nature et technologies. V. M. is funded by the

INCEPTION project [PIA/ANR-16-CONV-0005] and benefits from support from the CRI through "Ecole Doctorale FIRE – Programme Bettencourt". J.W. is supported by a Discovery grant from the Natural Sciences and Engineering Research Council of Canada.

References

- [1] Neocles B Leontis, Aurelie Lescoute, and Eric Westhof. The building blocks and motifs of rna architecture. *Current opinion in structural biology*, 16(3):279–287, 2006.
- [2] Neocles B Leontis and Eric Westhof. Geometric nomenclature and classification of rna base pairs. *Rna*, 7(4):499–512, 2001.
- [3] Sam Griffiths-Jones, Alex Bateman, Mhairi Marshall, Ajay Khanna, and Sean R Eddy. Rfam: an rna family database. *Nucleic acids research*, 31(1):439–441, 2003.
- [4] Aurelie Lescoute, Neocles B Leontis, Christian Massire, and Eric Westhof. Recurrent structural rna motifs, isostericity matrices and sequence alignments. *Nucleic acids research*, 33(8):2395–2409, 2005.
- [5] Mahassine Djelloul. *Algorithmes de graphes pour la recherche de motifs récurrents dans les structures tertiaires d'ARN*. PhD thesis, 2009.
- [6] Vladimir Reinharz, Antoine Soulé, Eric Westhof, Jérôme Waldispühl, and Alain Denise. Mining for recurrent long-range interactions in rna structures reveals embedded hierarchies in network families. *Nucleic acids research*, 46(8):3841–3851, 2018.
- [7] Anton I Petrov, Craig L Zirbel, and Neocles B Leontis. Automated classification of rna 3d motifs and the rna 3d motif atlas. *Rna*, 19(10):1327–1340, 2013.
- [8] Roman Sarrazin-Gendron, Vladimir Reinharz, Carlos G Oliver, Nicolas Moitessier, and Jérôme Waldispühl. Automated, customizable and efficient identification of 3d base pair modules with bayespairing. *Nucleic acids research*, 47(7):3321–3332, 2019.
- [9] James Roll, Craig L Zirbel, Blake Sweeney, Anton I Petrov, and Neocles Leontis. Jar3d webserver: Scoring and aligning rna loop sequences to known 3d motifs. *Nucleic acids research*, 44(W1):W320–W327, 2016.
- [10] Carlos Oliver, Vincent Mallet, Roman Sarrazin Gendron, Vladimir Reinharz, William L Hamilton, Nicolas Moitessier, and Jérôme Waldispühl. Augmented base pairing networks encode RNA-small molecule binding preferences. *Nucleic Acids Research*, 07 2020. gkaa583.
- [11] Grzegorz Chojnowski, Tomasz Waleń, and Janusz M Bujnicki. Rna bricks—a database of rna 3d motifs and their interactions. *Nucleic Acids Research*, 42(D1):D123–D131, 2014.
- [12] Ping Ge, Shahidul Islam, Cuncong Zhong, and Shaojie Zhang. De novo discovery of structural motifs in rna 3d structures through clustering. *Nucleic acids research*, 46(9):4783–4793, 2018.
- [13] Patrik D’haeseleer. What are dna sequence motifs? *Nature biotechnology*, 24(4):423–425, 2006.
- [14] Poul Nissen, Joseph A Ippolito, Nenad Ban, Peter B Moore, and Thomas A Steitz. Rna tertiary interactions in the large ribosomal subunit: the a-minor motif. *Proceedings of the National Academy of Sciences*, 98(9):4899–4903, 2001.
- [15] Peter W Rose, Andreas Prlić, Ali Altunkaya, Chunxiao Bi, Anthony R Bradley, Cole H Christie, Luigi Di Costanzo, Jose M Duarte, Shuchismita Dutta, Zukang Feng, et al. The rcsb protein data bank: integrative view of protein, gene and 3d structural information. *Nucleic acids research*, page gkw1000, 2016.
- [16] Zhiping Zeng, Anthony K. H. Tung, Jianyong Wang, Jianhua Feng, and Lizhu Zhou. Comparing stars: On approximating graph edit distance. *Proc. VLDB Endow.*, 2:25–36, 2009.
- [17] William L Hamilton, Rex Ying, and Jure Leskovec. Representation learning on graphs: Methods and applications. *arXiv preprint arXiv:1709.05584*, 2017.
- [18] Will Hamilton, Zhitao Ying, and Jure Leskovec. Inductive representation learning on large graphs. In *Advances in neural information processing systems*, pages 1024–1034, 2017.
- [19] Jesse Stombaugh, Craig L Zirbel, Eric Westhof, and Neocles B Leontis. Frequency and isostericity of rna base pairs. *Nucleic acids research*, 37(7):2294–2312, 2009.
- [20] Nino Shervashidze, SVN Vishwanathan, Tobias Petri, Kurt Mehlhorn, and Karsten Borgwardt. Efficient graphlet kernels for large graph comparison. In *Artificial Intelligence and Statistics*, pages 488–495, 2009.
- [21] H. W. Kuhn and Bryn Yaw. The hungarian method for the assignment problem. *Naval Res. Logist. Quart.*, pages 83–97, 1955.
- [22] Michael Schlichtkrull, Thomas N Kipf, Peter Bloem, Rianne Van Den Berg, Ivan Titov, and Max Welling. Modeling relational data with graph convolutional networks. In *European Semantic Web Conference*, pages 593–607. Springer, 2018.
- [23] Adam Paszke, Sam Gross, Francisco Massa, Adam Lerer, James Bradbury, Gregory Chanan, Trevor Killeen, Zeming Lin, Natalia Gimelshein, Luca Antiga, Alban Desmaison, Andreas Kopf, Edward Yang, Zachary DeVito, Martin Raison, Alykhan Tejani, Sasank Chilamkurthy, Benoit Steiner, Lu Fang, Junjie Bai, and Soumith Chintala. Pytorch: An imperative style, high-performance deep learning library. In H. Wallach, H. Larochelle, A. Beygelzimer, F. d’Alché Buc, E. Fox, and R. Garnett, editors, *Advances in Neural Information Processing Systems 32*, pages 8024–8035. Curran Associates, Inc., 2019.
- [24] Minjie Wang, Lingfan Yu, Da Zheng, Quan Gan, Yu Gai, Zihao Ye, Mufei Li, Jinjing Zhou, Qi Huang, Chao Ma, et al. Deep graph library: Towards efficient and scalable deep learning on graphs. *arXiv preprint arXiv:1909.01315*, 2019.
- [25] Xinbo Gao, Bing Xiao, Dacheng Tao, and Xuelong Li. A survey of graph edit distance. *Pattern Analysis and applications*, 13(1):113–129, 2010.
- [26] Horst Bunke and Kaspar Riesen. Graph classification based on dissimilarity space embedding. In *Joint IAPR International Workshops on Statistical Techniques in Pattern Recognition (SPR) and Structural and Syntactic Pattern Recognition (SSPR)*, pages 996–1007. Springer, 2008.
- [27] Cuncong Zhong and Shaojie Zhang. Rnamotifscanx: a graph alignment approach for rna structural motif identification. *RNA*, 21(3):333–346, 2015.
- [28] Laurens van der Maaten and Geoffrey Hinton. Visualizing data using t-sne. *Journal of machine learning research*, 9(Nov):2579–2605, 2008.

Appendix

1. RNA data

We present here the algorithm used to chop RNA into fixed maximal size pieces. The idea of the algorithm is to recursively cut the RNA in halves up until the maximum size is reached. This is detailed in **Algorithm 4**.

Algorithm 4: Chopper algorithm

Data: Full RNA Graph g , Maximum number of nodes N

Result: List of sub-structures of maximum size N .

```

37 if  $|g| \leq N$  then
38   | return
39 end
40  $g$ 
41 else
42    $g_a, g_b \leftarrow$  Split  $g$  in halves based on the PCA
43   axes
44   return chopper( $g_a$ )
45   return chopper( $g_b$ )
46 end

```

We include a representation of the notion of isostericity between edge types in **Figure A.8**.

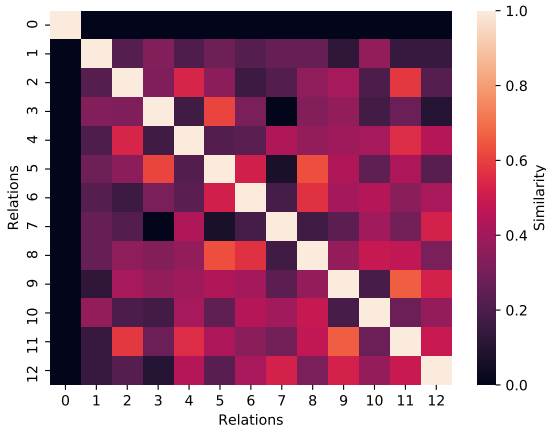


Figure A.8: Isostericity matrix between relation types.

2. Graph Edit Distance

The Graph Edit Distance (GED) between two graphs G and H is defined as follows:

$$GED(G, H) = \min_{(e_1, \dots, e_k) \in \Upsilon(G, H)} \sum_{i=1}^k c(o_i). \quad (4)$$

Where Υ is the set of all edit sequences which transform G into H . Edit operations include: node/edge matching, deletion, and insertion. $c(o)$ is the cost of performing edit operation o and c is known as the cost function. Since we will be decomposing our graphs as rooted subgraphs, we define a slight modification to

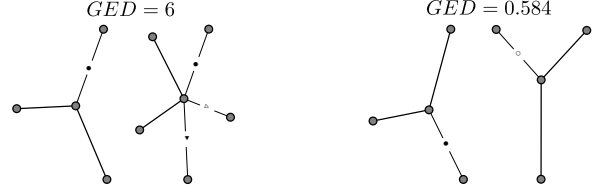


Figure A.9: Examples of similar and dissimilar pairs according to the GED A* algorithm.

the GED formulation which compares two graphs given that their respective roots must be matched to each other. This algorithm is detailed in **Algorithm 5**.

Algorithm 5: Rooted A* GED

Data:

- Pair of graphs G, H , (WLOG let G be the smaller of the two graphs.)
- cost function c
- heuristic h .
- $r_G \in \mathcal{N}(G)$ root in first graph
- $r_H \in \mathcal{N}(G)$ root in second graph

Result: Minimum cost rooted distance and alignment between two graphs.

```

47 OPEN  $\leftarrow$  priorityQueue()
48  $V_G \leftarrow G.nodes()$ 
49  $V_H \leftarrow H.nodes()$ 
50  $v \leftarrow$  first node in  $G$ 
   OPEN.add( $(r_G, r'_H), c(r_G, r_H) + h(v_0, v')$ ) while
   OPEN do
51    $v_{min} \leftarrow OPEN.pop()$ 
52   Let  $\mathcal{M}_k \leftarrow$  be partial mapping
      $\{(v_1, v'_1), \dots, (v_k, v'_k)\}$ 
53   if  $|\mathcal{M}_k| = |V_G|$  then
54     | Mapping complete
55     | return  $\mathcal{M}_k$ 
56   end
57   Add nodes at next depth
58   foreach  $u \in V_H \setminus v_{min}$  do
59     | OPEN.add( $v_{min} \cup (v_{k+1}, u), c(v_{k+1}, u) +$ 
60       |  $h(v_{k+1}, u)$ )
61   end

```

We include in **Figure A.9** an example of GED values for two pairs of graphlets, illustrating how similar graphs get lower values of distance.

3. Similarity Functions

3.1. Ring-based similarity functions. The first S functions we consider are a weighted sum of a distance between their l -hop neighborhoods (aka rings). We let $R_u = \{(u', w) : \delta(u, u') = l \ \forall (u', w) \in E\}$ be the set of edges at distance k from the root node u . Let d be a normalized similarity function between two sets

of edges. Let $0 < \lambda < 1$ be a decay factor to assign higher weight to rings closer to the root nodes, and N^{-1} be a normalization constant to ensure the function saturates at 1. Then we can obtain a structural similarity for the rooted subgraphs around u and v as :

$$k_L(u, v) := 1 - N^{-1} \sum_{l=0}^{L-1} \lambda^l d(R_u^l, R_v^l)$$

$$d(R_u, R_v) := \min - \sum_{e \in R_u} \sum_{e' \in R_v} \mathbf{S}_{\mathcal{L}(e), \mathcal{L}(e')} \mathbf{X}_{e, e'}$$

The first function (`R_1`) simply uses a delta function to compare to different edges. This assignment problem thus reduces to computing the intersection over union score between the histograms f_R of edge labels found at each ring. However, this function treats all edge types equally and ignore the isostericity relationships. The second function (`R_iso`) has a matching value of 1 for backbone edges matched with backbone edges, 0 for backbone matched with any non covalent bond and the isostericity value for the similarity value of two non covalent bond.

3.2. Matching Similarity Functions. In the ring-based similarity functions, comparisons only happen between rings at the same depth from the root. This can be a harsh constraint since two rooted subgraphs can have a similar global structure but the choice of root node can shift the rings to yield a very low similarity. For the matching functions, we allow matches to occur across all distances from the root with an additional cost matrix $\mathbf{D} \in \mathbb{R}^{\mathbb{R}}$, where $D_{i,j}$ contains the cost of matching elements whose distances to their roots are i and j ($= e^{-|i-j|}$). Instead of thinking of matching only the edges within a ring, we can think of matching tuples of edge labels and distances.

$E_u = \{(\mathcal{L}(u, w), d(u, w)) \mid \forall w \in G, d(u, w) \leq r\}$, where each element is a tuple composed of edge label and distance from the root for all nodes within the radius. Now the cost of matching a pair of edges is a function of their isostericity value as well as the distance between them.

$$d(E_u, E_v) := \min \sum_{e \in E_u} \sum_{e' \in E_v} (\alpha \mathbf{S}_{\mathcal{L}(e), \mathcal{L}(e')} + \beta \mathbf{D}_{e, e'}) \mathbf{X}_{e, e'} \quad (5)$$

3.3. Graphlet similarity functions. We can generalize the edge ring similarity function by considering the neighborhood of a node to consist of a multi-set of smaller graphs (known as graphlets) instead of simply edge labels. This allows us to consider more complex structural features than sets of edge labels allows for. Since the degree of our graphs is strongly bounded (max degree 5), we can define a graphlet as a rooted subgraph of radius 1 and obtain a manageable number of possible graphlets. Moreover the rooted aspect and the small size of those graphs make the GED computation tractable. We can then make an analogy between graphlet identity and edge type to obtain the same formulation and solution as the edge similarity function.

While the GED computation is tractable for such small graphs, it is still expensive when repeated many times. For this reason, we implement a solution caching strategy which stores the computed GED when it sees a new pair of graphlets, and looks up stored solutions when it recognizes a previously seen pair **Supplementary Algorithm 6**.

We can now define \mathbf{S} from Equation 1 as $\mathbf{S}_{ij} = \exp[-\gamma \text{GED}(g_i, g_j)]$. We apply an exponential to the distance to bring the distances to the range [0,1], and convert them to a similarity. An optional scaling parameter γ is included to control the similarity penalty on more dissimilar graphs. We also note

that the construction of \mathbf{S} can be parallelized but we leave the implementation for future work.

3.4. Additional settings. We have experimented with several additional parameters. We tried including an Inverse Document Frequency (IDF) weighting to account for the higher frequency of non canonical interaction. This amounted to scale all comparison value by the product of the IDF term they involved.

We also tried adding a re-normalization scheme to give higher values to matches of long rings. In particular, we want to express that a having a match of 9 out of 10 elements is stronger than having a match of 2 out of 3. Let S be the raw matching score, \mathbb{S} the normalized one and L be the length of the sequences, we have tried two normalization settings, the ‘‘sqrt’’ and ‘‘log’’ ones :

$$\text{sqrt} : \mathbb{S} = \left[\frac{S}{L} \right]^{\frac{5}{\sqrt{L}}}$$

$$\text{log} : \mathbb{S} = \left[\frac{S}{L} \right]^{\frac{1}{1+\log L}}$$

4. Graphlets hashing and distributions

To do this, we build a hash function which maps isomorphic graphlets to the same output, while assigning different outputs to non-isomorphic ones, allowing us to look up graphlet GED values. This is done by building a sparse representation of an explicit Weisfeiler-Lehman isomorphism kernel, with a twist that edge labels are included in the neighborhood aggregation step. The resulting hash consists of counts over the whole graphlet of hashed observed sequences of edge labels. We enforce the edge label hashing function to be permutation invariant by sorting the observed label sequence. In this manner, isomorphic graphs are given identical hash values regardless of node ordering. Our hashing procedure outlined in **Supplemental Algorithm 6** also allows us to study the distribution of graphlets composing RNA networks **Supplemental Fig A.10**, where we can observe a characteristic power law distribution.

Algorithm 6: Weisfeiler-Lehman Edge Graphlet Hashing

Data:

- Graphlet g ,
- Maximum depth K
- HASH, function from strings to integers
- \mathcal{L} function returning the label for an edge

Result: Hash code for graphlet h

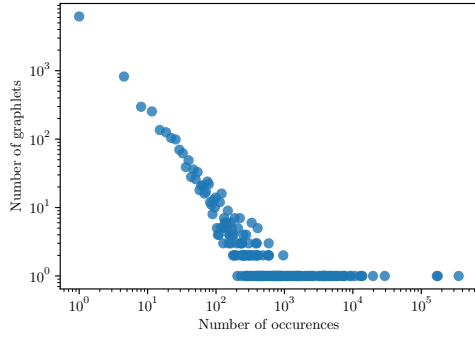
```

62  $h \leftarrow \text{counter}()$ 
63 foreach  $k \in \{1, \dots, K\}$  do
64   foreach  $u \in g_N$  do
65      $l_u^k \leftarrow \text{HASH}(\{\mathcal{L}(u, v) \oplus l_v^{k-1} \mid \forall v \in \mathcal{N}(u)\})$ 
66   end
67    $h \leftarrow h \cup \text{counter}(\{l_u \mid \forall u \in g\})$ 
68 end
69 return  $h$ 

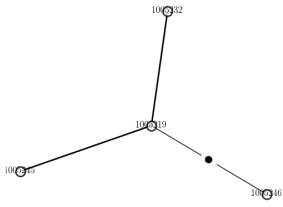
```

5. Structural clusters

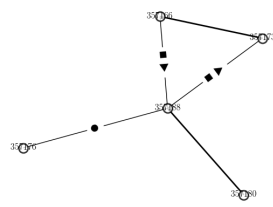
We present in **Figure A.11** some metrics on the clustering of our structural embeddings. We see that these metrics suggest that the structures present in RNA do fall into well separated clusters.



(a) Graphlet frequency distribution

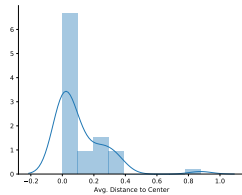


(b) Most frequent graphlet

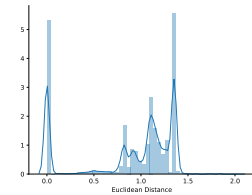


(c) Example of a rare graphlet.

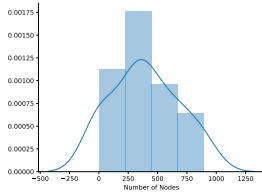
Figure A.10: Graphlet distribution and examples.



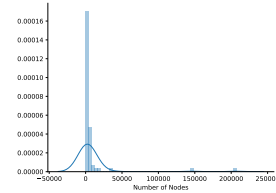
(a) Average distance to center.



(b) Distance between randomly selected pairs of embeddings.



(c) Number of nodes per cluster (removing clusters with more than 5000 nodes)



(d) Nodes per cluster, unfiltered.

Figure A.11: Clustering K-means $k = 262$

6. Retrieve complexity

In this section, we want to investigate the complexity of the retrieve algorithm. This complexity depends highly on both the topology of the meta-graph, the query graph and the individual RNA-graphs.

Let N_p be the number of edges in each of the p parallel edges of the query graph, and E_p be the corresponding meta-edge. We consider the edges of the query graph in the order of the parallel edges, let $p(t) = \min_k, \sum_k N_k > t$, the parallel edge considered at time t .

At each step t , the complexity bound is going to depend on the number of candidate motifs inside each RNA graphs at time $t-1$ as well as the number of possible additional edges to insert into those candidates. If we denote as $M_{g,t}$ the number of candidates in graph g at time t , and $N_{g,t}$ the number of edges in graph g that belong to the meta-edge $E_{p(t),g}$, the complexity writes as $O(\sum_t \sum_{g \in \mathcal{G}} E_{p(t),g} M_{g,t})$. The term $E_{p(t),g}$ mostly acts as a sparsity term, as it would not exceed ten but can very often be zero if the graph does not include such an edge. Therefore, we introduce the notation \mathcal{G}_p , the set of RNA graphs that contain an edge in E_p , to omit this term. We also introduce $t_{g,t} = \sum_{l < t} E_{p(l),g}$ the number of query edges explored present in graph g at time t .

Let us now try to address the second term $M_{g,t}$. We divide our algorithm into each of the parallel edges and dive into the evolution of this term. $M_{g,t}$ represents the number of combinations of nodes in a given graph that are currently considered as a candidate motif. Every different p is going to launch a combinatorial explosion that results from the numerous possibilities of combining nodes. For RNA graphs, it is mostly a problem for stems that are ubiquitous and all share the same structure. Starting from all stem nodes, after one merging step we have to add all possible combinations of adjacent stem nodes. We give a loose bound of this number that is practical for our application, but note that after sufficient merging, there are just the full stems as candidates, showing that this bound becomes loose.

We rely on the fact that we can delete a partial solution if it is completely contained into another one because its expansion can only result in lower scores. Thus after a given motif got expanded we can remove it from \mathcal{M} . Therefore, we can bound this number by counting the number of children a given element can produce. Using sets structure enables fast neighborhood checking operations but also ensures we do not add the same object twice. For stems that are the worst case scenario, each connected component of length k can yield a maximum of $k + 2$ children but any of this children is added twice because the edge has two ends. Therefore after k expansions, we have $M_{g,t+k} < M_{g,t} \frac{(k+2)!}{2^k}$. This results in a final loose complexity bound of: $O(\sum_t \sum_{g \in \mathcal{G}_{p(t)}} \frac{(t_{g,t}+2)!}{2^{t_{g,t}}})$.

As mentioned before this is not a good bound when k grows because the stems get completed. Therefore, there are a lot of ways to select 3 adjacent stem nodes of a 6 stem, but only one to get all 6. In practice, during each cycle, the number $M_{g,t}$ grows and decreases, making the algorithm tractable, starting back from reasonable numbers at each cycles. Empirically, running the retrieve algorithm on a single core rarely exceed a few seconds.

7. Full results for the similarity function validations

We include in this section the full results we got for a grid search validation in the absence of a better way to guide our intuition.

| method | depth | decay | normalization | r_exp | r_threshold | r_nc | r_nc_threshold | time |
|-------------|-------|-------|---------------|-------|-------------|-------|----------------|-------|
| R_1 | 1 | 0.500 | None | 0.630 | 0.630 | 0.386 | 0.397 | 0.000 |
| R_1 | 1 | 0.500 | sqrt | 0.630 | 0.630 | 0.386 | 0.397 | 0.000 |
| R_1 | 1 | 0.300 | None | 0.630 | 0.630 | 0.386 | 0.397 | 0.000 |
| R_1 | 1 | 0.800 | sqrt | 0.630 | 0.630 | 0.386 | 0.397 | 0.000 |
| R_1 | 1 | 0.300 | sqrt | 0.630 | 0.630 | 0.386 | 0.397 | 0.000 |
| R_1 | 1 | 0.800 | None | 0.630 | 0.630 | 0.386 | 0.397 | 0.000 |
| R_1 | 1 | 0.800 | sqrt | 0.633 | 0.627 | 0.320 | 0.334 | 0.000 |
| R_1 | 1 | 0.500 | None | 0.633 | 0.627 | 0.320 | 0.334 | 0.000 |
| R_1 | 1 | 0.800 | None | 0.633 | 0.627 | 0.320 | 0.334 | 0.000 |
| R_1 | 1 | 0.500 | sqrt | 0.633 | 0.627 | 0.320 | 0.334 | 0.000 |
| R_1 | 1 | 0.300 | sqrt | 0.633 | 0.627 | 0.320 | 0.334 | 0.000 |
| R_1 | 1 | 0.300 | None | 0.633 | 0.627 | 0.320 | 0.334 | 0.000 |
| hungarian | 1 | NaN | sqrt | 0.726 | 0.732 | 0.474 | 0.482 | 0.001 |
| R_iso | 1 | 0.800 | sqrt | 0.757 | 0.758 | 0.494 | 0.503 | 0.000 |
| R_iso | 1 | 0.500 | sqrt | 0.757 | 0.758 | 0.494 | 0.503 | 0.000 |
| R_iso | 1 | 0.300 | sqrt | 0.757 | 0.758 | 0.494 | 0.503 | 0.000 |
| hungarian | 1 | NaN | sqrt | 0.758 | 0.764 | 0.527 | 0.530 | 0.001 |
| R_iso | 1 | 0.300 | sqrt | 0.758 | 0.760 | 0.510 | 0.515 | 0.000 |
| R_iso | 1 | 0.500 | sqrt | 0.758 | 0.760 | 0.510 | 0.515 | 0.000 |
| R_iso | 1 | 0.800 | sqrt | 0.758 | 0.760 | 0.510 | 0.515 | 0.000 |
| R_iso | 1 | 0.500 | None | 0.768 | 0.777 | 0.467 | 0.483 | 0.000 |
| R_iso | 1 | 0.300 | None | 0.768 | 0.777 | 0.467 | 0.483 | 0.000 |
| R_iso | 1 | 0.800 | None | 0.768 | 0.777 | 0.467 | 0.483 | 0.000 |
| R_iso | 1 | 0.800 | None | 0.769 | 0.783 | 0.526 | 0.533 | 0.000 |
| R_iso | 1 | 0.300 | None | 0.769 | 0.783 | 0.526 | 0.533 | 0.000 |
| R_iso | 1 | 0.500 | None | 0.769 | 0.783 | 0.526 | 0.533 | 0.000 |
| hungarian | 1 | NaN | None | 0.790 | 0.799 | 0.488 | 0.499 | 0.001 |
| hungarian | 1 | NaN | None | 0.791 | 0.800 | 0.612 | 0.612 | 0.000 |
| R_graphlets | 1 | 0.300 | sqrt | 0.940 | 0.942 | 0.890 | 0.894 | 0.029 |
| R_graphlets | 1 | 0.800 | sqrt | 0.940 | 0.942 | 0.890 | 0.894 | 0.029 |
| R_graphlets | 1 | 0.500 | sqrt | 0.940 | 0.942 | 0.890 | 0.894 | 0.029 |
| R_graphlets | 1 | 0.500 | None | 0.967 | 0.973 | 0.948 | 0.962 | 0.029 |
| R_graphlets | 1 | 0.300 | None | 0.967 | 0.973 | 0.948 | 0.962 | 0.029 |
| R_graphlets | 1 | 0.800 | None | 0.967 | 0.973 | 0.948 | 0.962 | 0.029 |
| graphlet | 1 | NaN | None | 0.967 | 0.973 | 0.948 | 0.962 | 0.030 |
| graphlet | 1 | NaN | sqrt | 0.996 | 0.997 | 0.992 | 0.995 | 0.030 |

TABLE A.5: One hop correlation to GED

| method | depth | decay | normalization | r_exp | r_threshold | r_nc | r_nc_threshold | time |
|-------------|-------|-------|---------------|-------|-------------|-------|----------------|-------|
| R_l | 2 | 0.300 | None | 0.375 | 0.444 | 0.241 | 0.328 | 0.000 |
| R_l | 2 | 0.300 | sqrt | 0.375 | 0.444 | 0.241 | 0.328 | 0.000 |
| R_l | 2 | 0.300 | sqrt | 0.381 | 0.440 | 0.246 | 0.315 | 0.000 |
| R_l | 2 | 0.300 | None | 0.381 | 0.440 | 0.246 | 0.315 | 0.000 |
| R_iso | 2 | 0.300 | None | 0.385 | 0.469 | 0.236 | 0.336 | 0.000 |
| R_iso | 2 | 0.300 | None | 0.402 | 0.481 | 0.233 | 0.337 | 0.000 |
| R_graphlets | 2 | 0.300 | None | 0.405 | 0.462 | 0.314 | 0.378 | 0.352 |
| R_l | 2 | 0.500 | sqrt | 0.407 | 0.480 | 0.264 | 0.356 | 0.000 |
| R_l | 2 | 0.500 | None | 0.407 | 0.480 | 0.264 | 0.356 | 0.000 |
| R_iso | 2 | 0.500 | None | 0.412 | 0.511 | 0.259 | 0.376 | 0.000 |
| R_iso | 2 | 0.300 | sqrt | 0.414 | 0.490 | 0.259 | 0.343 | 0.000 |
| R_l | 2 | 0.500 | None | 0.416 | 0.477 | 0.276 | 0.351 | 0.000 |
| R_l | 2 | 0.500 | sqrt | 0.416 | 0.477 | 0.276 | 0.351 | 0.000 |
| R_iso | 2 | 0.300 | sqrt | 0.416 | 0.492 | 0.256 | 0.344 | 0.000 |
| R_graphlets | 2 | 0.500 | None | 0.429 | 0.496 | 0.334 | 0.406 | 0.356 |
| R_iso | 2 | 0.500 | None | 0.434 | 0.525 | 0.261 | 0.385 | 0.000 |
| R_l | 2 | 0.800 | None | 0.438 | 0.516 | 0.285 | 0.382 | 0.000 |
| R_l | 2 | 0.800 | sqrt | 0.438 | 0.516 | 0.285 | 0.382 | 0.000 |
| R_iso | 2 | 0.800 | None | 0.438 | 0.551 | 0.280 | 0.416 | 0.000 |
| R_iso | 2 | 0.500 | sqrt | 0.451 | 0.540 | 0.288 | 0.391 | 0.000 |
| R_l | 2 | 0.800 | None | 0.451 | 0.515 | 0.304 | 0.387 | 0.000 |
| R_l | 2 | 0.800 | sqrt | 0.451 | 0.515 | 0.304 | 0.387 | 0.000 |
| R_iso | 2 | 0.500 | sqrt | 0.454 | 0.543 | 0.286 | 0.395 | 0.000 |
| hungarian | 2 | NaN | None | 0.455 | 0.620 | 0.292 | 0.499 | 0.001 |
| R_graphlets | 2 | 0.800 | None | 0.456 | 0.535 | 0.356 | 0.437 | 0.357 |
| R_iso | 2 | 0.800 | None | 0.465 | 0.568 | 0.288 | 0.434 | 0.000 |
| graphlet | 2 | NaN | None | 0.470 | 0.574 | 0.347 | 0.462 | 0.430 |
| R_iso | 2 | 0.800 | sqrt | 0.488 | 0.589 | 0.316 | 0.440 | 0.000 |
| hungarian | 2 | NaN | None | 0.491 | 0.622 | 0.261 | 0.437 | 0.001 |
| R_iso | 2 | 0.800 | sqrt | 0.493 | 0.593 | 0.316 | 0.445 | 0.000 |
| R_graphlets | 2 | 0.300 | sqrt | 0.505 | 0.533 | 0.405 | 0.417 | 0.353 |
| hungarian | 2 | NaN | sqrt | 0.533 | 0.666 | 0.320 | 0.521 | 0.001 |
| R_graphlets | 2 | 0.500 | sqrt | 0.543 | 0.576 | 0.444 | 0.459 | 0.356 |
| hungarian | 2 | NaN | sqrt | 0.554 | 0.686 | 0.277 | 0.472 | 0.001 |
| graphlet | 2 | NaN | sqrt | 0.568 | 0.637 | 0.437 | 0.518 | 0.433 |
| R_graphlets | 2 | 0.800 | sqrt | 0.587 | 0.626 | 0.487 | 0.506 | 0.356 |

TABLE A.6: Two hop Correlation

| Motif Size | Number of Motifs | Mean Number of Instances |
|------------|------------------|--------------------------|
| 1 | 50 | 3875.02 |
| 2 | 240 | 1804.80 |
| 3 | 73 | 1601.21 |
| 4 | 115 | 2071.23 |
| 5 | 426 | 928.37 |
| 6 | 761 | 469.72 |

TABLE A.7: Number of motifs and of instances per motif for each size, as found by the MAGA algorithm